JOURNAL OF PROPULSION AND POWER
Vol. 18, No. 1, January–February 2002

Analytical Model of the Base Flow Between a Subsonic and Supersonic Flow

Doo S. Baik*
Kookmin University, Seoul 136-702, Republic of Korea
and
Glen W. Zumwalt†
Wichita State University, Wichita, Kansas 67260

A flow-modeling method has been developed to analyze the flow in the annular base (rear-facing surface) of a circular engine nacelle flying at subsonic speed but with a supersonic exhaust jet. Real values of exhaust gas properties and temperature are included. Potential flows of the air and gas streams are computed for the flow past a separated wake. Then a viscous jet mixing is superimposed on this inviscid solution. Conservation of mass, momentum, and energy is achieved by multiple iterations. Despite the iterations, the wake flowfield is computed with modest computer requirements.

Nomenclature

C_p = pressure coefficient
Cr = Crocco number, $U/U_{\max}$
c_p = specific heat
D = distance of the body extends upstream from the base
E = distance of the downstream from recombination point
$E(k)$ = second elliptical integral
H = height of the base
h = enthalpy
I, J = integrals
$K(k)$ = first elliptical integral
L = length wake extends from the base
P = pressure
Pr = Prandtl number
R = radius from nacelle axis
$\dot{R}_i$ = radius of computation ring
$\dot{R}_j$ = radius of singularity ring
$\Re$ = gas constant
T = temperature
U, V = velocity components
X, R = axisymmetric coordinates (X–R)
X, Y = reference inviscid coordinates (X–Y)
X_0 = axial distance of virtual origin from separation point
x, y = coordinates fixed to the jet mixing region
Y_0 = normal distance of virtual origin from separation point
y_m = shift of x axis from X axis
α = Mach angle, $\sin^{-1}(M^{-1})$
β = $\sqrt{(1 - M_\infty^2)}$
γ = ratio of specific heats; vortex strength
δ = boundary-layer thickness
δ_1 = boundary-layer displacement thickness
δ_2 = boundary-layer momentum thickness
η = dimensionless y coordinates
θ = flow angle from body axis
μ = ring source strength
ρ = density
σ = jet mixing spreading parameter
Φ = velocity ratio, u/U_e
Ω = variable in first/second elliptic integrals
ω = surface angle from the axis

Subscripts

B, B' = back flow value
b = base region value
e, e' = adjacent inviscid streamline
i = control point number
J = exhaust jet
j = singularity ring number
R = radial direction
r = streamline r
s = source; streamline s
t = turbulent flow
v = vortex
X = axial direction
0 = stagnation condition

Superscripts

n = normal velocity component
t = tangential velocity component
$\cdot$ = incompressible flow
$'$ = supersonic flow side
$-$ = average value

Received 17 November 2000; revision received 6 August 2001; accepted for publication 8 August 2001.

*Research Assistant/Professor, Graduate School of Automotive Engineering, 861-1 Chongnung-dong, Songbuk-gu; dsbaik@kookmin.ac.kr. Member AIAA.
†Distinguished Emeritus Professor, National Institute for Aviation Research, 1845 Fairmount; gzcz@juno.com. Member AIAA.

I. Introduction

FOR decades, there has been considerable interest in understanding and predicting the characteristics of aircraft afterbody flow. In the beginning of such research, only experimental methods were available. Because the experimental studies could be quite complex and expensive, there has been considerable interest in developing less expensive, yet reliable, analytical and numerical schemes. For the most accurate results, the full Navier–Stokes equations should be solved using a finite difference method, but this requires a large computer and long computational time. Holst[1] first solved the Navier–Strokes equations for supersonic flows over axisymmetric boattails with a solid plume simulator. Mikhail[2] removed the solid plume simulator and considered a centered propulsive jet emanating from a sharp lipped nozzle at a Mach number of one. Peery and Forester[3] treated multistream nozzle flows with transonic external flow and a central jet with exit area equal to the body area.

Deiwert[4] used an implicit method to simulate subsonic, transonic, and supersonic three-dimensional separated flows over axisymmetric boattailed bodies with a solid plume simulator. Hasen[5] obtained numerical solution for an axisymmetric nozzle in supersonic external flowfield using MacCormack's method.

All of the cited authors used finite difference techniques. In this, a large portion of the enveloping flowfield must be computed point by point to find the pressure in a small region. This requires thousands of computational points. Singularity methods require only that flow conditions on the body (or jet) surface be computed.

Korst and Tripp[6] investigated the base pressure behind a blunt trailing edge for supersonic two-dimensional flow in which two approaching streams on each side of the trailing edge have the same composition, constant specific heats, and identical stagnation temperature, but different Mach number and stagnation pressures. Page and Korst[7] developed the constant pressure freejet mixing of a turbulent supersonic plane backstep flow with a supersonic atmospheric flow of the same gas but different total temperature from the wake. Later, Korst's two-stream theoretical base flow analysis was extended to treat base flow on an axisymmetric afterbody with single operating exhaust nozzle by Dixon and Page.[8] In this both the airflow and nozzle flow were supersonic with the same gases.

Before Izadi,[9] no work can be found in which the outer flow is subsonic and the inner supersonic, despite the frequent occurrence in engine nacelles. Izadi modeled a base region between a subsonic and a supersonic flow to see if a singularity representation could be used with plane geometry, same gases, and same total temperatures.

The current research development follows the efforts of Izadi, where base flow due to internal supersonic and external subsonic flows was considered. Furthermore, the propulsion base flow was simplified by the assumptions of two-dimensional flow, air for both flows, and equal total temperatures. In the current investigation, an axisymmetric method of characteristics is used to simulate the supersonic wake region.

In the large body of analytical and computational work done on base flow, one commonly occurring case seems to have been overlooked: an axisymmetric aircraft nacelle with a hot supersonic exhaust gas jet interacting with a subsonic external flow of atmospheric air. This may occur in several ways; some are shown in Fig. 1.

In Fig. 1a, airflow separates from a boattail due to an adverse pressure gradient, creating an annulus. In Fig. 1b, separation is caused by the termination of the exterior surface. In Fig. 1c, a rocket is shown during acceleration to sonic speed. The time for which this occurs may be short, but the area on which base pressure prevails is large. Cooling airflow may be added to the annulus in Figs. 1a and 1b especially for turbojets with afterburners.

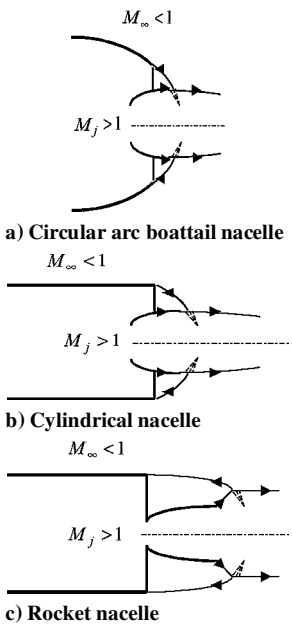

Fig. 1 Typical occurrence of axisymmetric base flows.

A flow-modeling approach, rather than finite difference method, was used to produce a solution that is economical enough in computer time to be useful for aircraft design. Singularities are used for the inviscid/subsonic airflow and the axisymmetric method of characteristics is used for the supersonic flow. Realistic gas properties can be specified. To the potential flows thus produced are added the viscous boundary layers and viscous jet interactions using the Chapman–Korst jet mixing method.

II. Model

The mathematical model involves an interactive solution between an outer, inviscid, potential flow and an inner, viscous flow in the near wake. The outer flow includes the subsonic airflow and the supersonic engine exhaust. These flow around the solid nacelle and the base wake. The inner solution then imposes viscous jet mixing and recirculation flows on the external flow. Satisfaction of mass, momentum, and energy conservation is achieved by interactive adjustment of the two flows.

It is typical of flow modeling methods to use knowledge of physical behaviors to simplify the analysis. Prandtl was perhaps the master of this when he proposed the boundary layer in which terms were eliminated on the basis of relative magnitudes and regions were labeled inviscid or viscous. Similarly, the pressure field patterns for separating and reattaching flow can be seen in many measured flows.

Based on general knowledge of base flows, a pressure field shape is assumed. Pressure in the wake is assumed to be a function of x, the axial position, only; therfore, pressures are equal on the upper and lower edges of the wake. The base pressure P_b prevails for about half of the axial length of the wake, L, then P rises to a maximum P_{rec}, near the point where the two outer flows combine, then slowly decreases to atmospheric pressure downstream. The general shape of P vs x curve is, thus, assumed, but the values of P_b and P_{rec} are produced by the computation.

A. Outer Flow Model

The subsonic potential flow is produced by adding to the atmospheric freestream the perturbations due to ring sources and vortices. The flow is transformed to the incompressible plane for solution, then transformed back to the compressible plane.

Goethert's rule,[10] where the dot denotes the incompressible case, is as follows:

$$\dot{X} = X, \qquad \dot{\omega} = \beta\omega, \qquad C_p = (1/\beta^2)\dot{C}_p, \qquad U_\infty = \dot{U}_\infty$$

where

$$\beta = \sqrt{1 - M_\infty^2}$$

Rings were distributed axially and the midpoints between rings were the computation points. The velocities resulting from the freestream and the singularities were added to give the velocity components,

$$\dot{U}_X = \dot{U}_\infty + \dot{U}_{sX} + \dot{U}_{vX}, \qquad \dot{U}_R = \dot{U}_{sR} + \dot{U}_{vR}$$

where[11]

$$\dot{U}_{sX} = \sum_{j=1}^{N+1} \left[\frac{\mu}{2\pi r_j'} \frac{2x}{\sqrt{x^2 + (r+1)^2}\{x^2 + (r-1)^2\}} E(k) \right]_j$$

$$\dot{U}_{sR} = \sum_{j=1}^{N+1} \left(\frac{\mu}{2\pi r_j'} \frac{1}{r\sqrt{x^2 + (r+1)^2}} \times \left[K(k) - \left\{ 1 - \frac{2r(r-1)}{x^2 + (r-1)^2} \right\} E(k) \right] \right)_j$$

$$\dot{U}_{vX} = \sum_{j=1}^{N+1} \left(\frac{\gamma}{2\pi r'_j} \frac{1}{\sqrt{x^2 + (r+1)^2}} \times \left[K(k) - \left\{ 1 + \frac{2(r-1)}{x^2 + (r-1)^2} \right\} E(k) \right] \right)_j$$

$$\dot{U}_{vR} = \sum_{j=1}^{N+1} \left(\frac{\gamma}{2\pi r'_j} \frac{-x}{r\sqrt{x^2 + (r+1)^2}} \times \left[K(k) - \left\{ 1 + \frac{2r}{x^2 + (r-1)^2} \right\} E(k) \right] \right)_j$$

where

$$k^2 = \frac{4r}{x^2 + (r+1)^2}, \qquad K(k) = \int_0^{\pi/2} \frac{1}{\sqrt{1 - k^2 \sin^2 \Omega}} \, d\Omega$$

$$E(k) = \int_0^{\pi/2} \sqrt{1 - k^2 \sin^2 \Omega} \, d\Omega, \qquad r = \frac{\dot{R}_i}{\dot{R}_j}$$

$$r'_j = \dot{R}_j, \qquad x = \frac{\dot{X}_j - \dot{X}_i}{\dot{R}_j}$$

The velocity components at a control point i, tangential and normal to the ith surface between rings, can be obtained by means of the following transformation where ω is the surface angle:

$$\begin{bmatrix} \dot{U}_i^t \\ \dot{U}_i^n \end{bmatrix} = \begin{bmatrix} \cos\omega_i & \sin\omega_i \\ -\sin\omega_i & \cos\omega_i \end{bmatrix} \begin{bmatrix} \dot{U}_X \\ \dot{U}_R \end{bmatrix}$$

Figure 2 shows the four regions with different boundary conditions to be applied for the outer flow.

1) At the region $1 \le i \le N1$, there are $(N1)$ rings over the body, starting at a point on the cylinder upstream (ring 1) having freestream flow and ending at the separating ring $(N1)$. For a control point i on this fixed surface, the normal velocities are

$$\dot{U}_i^n \big/ \dot{U}_\infty = 0, \qquad 0 \le X \le D$$

2) At the region $N1 + 1 \le i \le N2$, for a control point i on the flow surface between (ring $N1$) and the ring at the middistance of the wake (ring $N2$), the surface velocity at a control points is a function of base pressure:

$$\frac{\dot{U}_i^t}{\dot{U}_\infty} = \beta \frac{U_i^t}{U_\infty} = \beta \frac{U_b}{U_\infty}, \qquad D \le X \le \left(D + \frac{L}{2} \right)$$

where

$$\frac{U_b}{U_\infty} = \sqrt{1 + \frac{1}{M_\infty^2} \frac{2}{\gamma - 1} \left[1 - \left(\frac{p_b}{p_\infty} \right)^{(\gamma-1)/\gamma} \right]}$$

3) At the region $N2 \le i \le N3$, for a control point i on the flow surface between the (ring $N2$) and the ring at the end of the wake (recombination $N3$), considering an assumption of quadratic pressure rise, the surface velocity at these points are calculated from the following:

$$\frac{\dot{U}_i^t}{\dot{U}_\infty} = \beta \frac{U_i^t}{U_\infty} = \beta \left[\frac{4}{3} \left(\frac{U_{\text{rec}}}{U_\infty} - \frac{U_b}{U_\infty} \right) \left(\frac{X}{L} \right)^2 - \frac{1}{3} \left(\frac{U_{\text{rec}}}{U_\infty} - 4 \frac{U_b}{U_\infty} \right) \right]$$

for

$$\left(D + \frac{L}{2} \right) \le X \le (D + L)$$

where

$$\frac{U_{\text{rec}}}{U_\infty} = \sqrt{1 + \frac{1}{M_\infty^2} \frac{2}{\gamma - 1} \left[1 - \left(\frac{p_{\text{rec}}}{p_\infty} \right)^{(\gamma-1)/\gamma} \right]}$$

4) At the region $(N3 + 1) \le i \le N$, considering the rings between the end of the wake and some ring far downstream of the body and assuming that the flow over these rings are parallel to the flow surface, that is, the normal velocity is equal to zero, the surface velocity at the control point of the rings is

$$\dot{U}_i^n \big/ \dot{U}_\infty = 0, \qquad (D + L) \le X \le (D + L + E)$$

There are $(N + 1)$ rings with N control points over the body, the wake surface, and after the wake (subsonic side). Where it is assumed that there is no discontinuity between vortices, there are $2N + 1$ unknowns (source rings and vortex rings) and N equations. Two assumptions can be made to reduce the unknowns.

1) The source rings are all of equal strength.

2) The first ring is sufficiently far upstream that its tangential velocity is equal to the freestream velocity.

The outer potential flow can now be produced as follows. First, initial guesses are made for base pressure, recombination pressure, wake shape (regions 2 and 3), and streamline shape downstream of the recombination point (region 4). Expected pressures are

$$P_{0\infty} > P_{\text{rec}} > P_b$$

The program computes the velocities and changes the wake shape to reduce the normal velocities to zero.

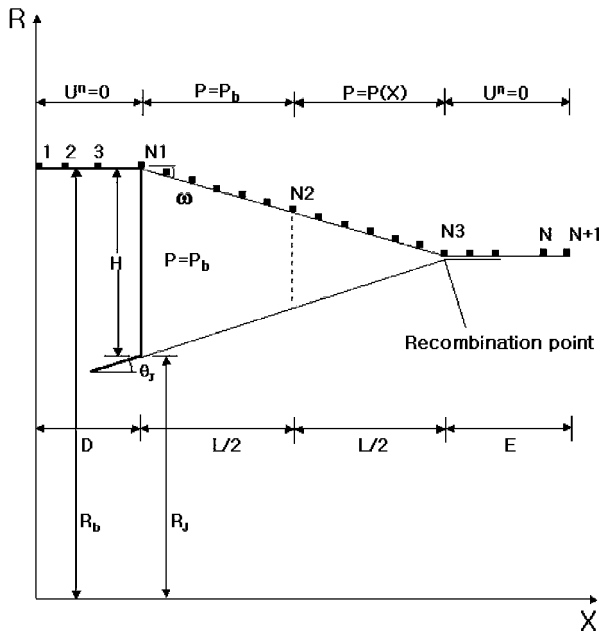

Fig. 2 Boundary conditions representation on body and wake.

B. Jet Flow Model

Symbols referring to the jet flow are indicated by a prime. The supersonic jet flow is computed by the axisymmetric method of characteristics[10] because singularity solutions are quite difficult for supersonic flow. In addition, the method of characteristics can approach exactness if small increments are used.

The pressure field choices are the same as those made for the subsonic outer flow. The streamlines at the end of the wake should join. If they cross, the chosen base pressure is too low. If they fail to join, the base pressure was chosen too high. A new value is chosen, and the two calculations are repeated until they join at the recombination point.

Downstream of the recombination point, the two streamlines should flow together (parallel) and have the same pressures. If this is not the case, the program moves the streamlines toward to lower pressure side, and the two solutions are again calculated with the new downstream geometry. When the wake shapes have relaxed, the upper and lower streamlines meet at a point and flow downstream at the same directions and pressures, and the outer, inviscid computation is completed.

Figure 3 shows schematically the upper portion of the region where a jet of compressible fluid discharges into atmosphere having certain pressure P. At a point on the outer boundary of the jet, denoted as point 4, the static pressure is known. Accordingly, the numerical procedure for analyzing a given pressure boundary point must take into account the condition $P_4 =$ known.

An initial value line must be established for initiating the calculation of the downstream supersonic flowfield. Because the static pressure of the exhaust gas at the exit lip exceeds that of the surrounding pressure, a Prandtl–Meyer expansion occurs at the exit lip point. Figure 4 shows the process for determining the right-running characteristics emanating at specified turning angles from the exit lip point. The flow properties at point 1 are determined by applying the Prandtl–Meyer expansion wave analysis, and the interior point process may then be employed for determining the location and the flow properties at point 4. The initial value line shown assumes that the nozzle flow is perfectly expanded so that the flow properties are uniform. This may not be true, but the flowfield exiting from the nozzle should be known. Then the method of characteristics computation would begin at the separation corner and proceed inward.

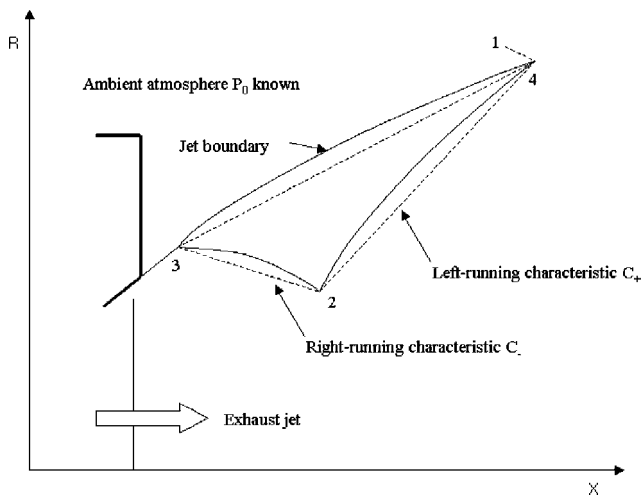

Fig. 3 Unit process for a jet boundary.

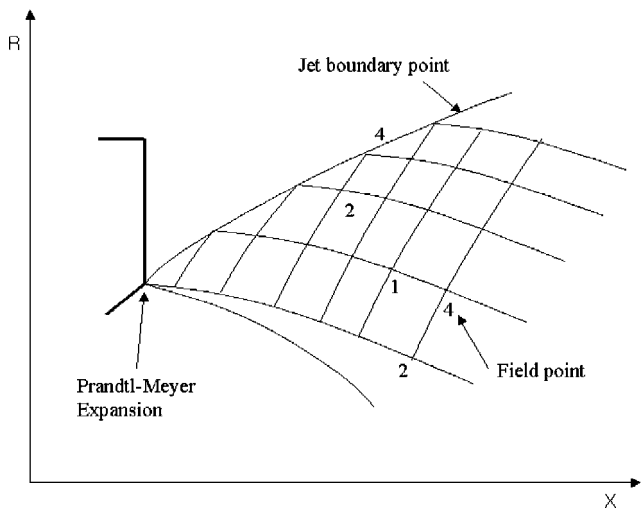

Fig. 4 Prandtl–Meyer expansion unit process.

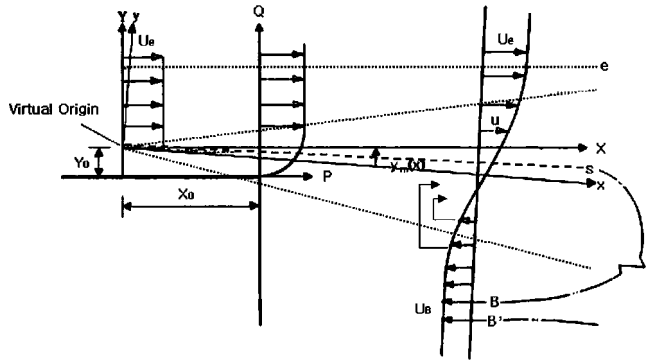

Fig. 5 Basic flow model of the two stream jet mixing.

If a shock pattern exists in the exhaust flow, this would be more complicated. Tam et al.[12] offer techniques for treating imperfectly expanded jets. However, the base flow region is usually relatively short and exhaust shocks will likely exert influence downstream of it.

C. Inner Flow Model

The analysis of the viscous flow within the wake is called the inner flow solution. It is based on Korst's turbulent-jet-mixing theory[13] and base flow analysis. This is modified to include a reverse flowing parallel stream and variable fluid properties. Korst's mixing theory, which has strong experimental verification, includes two fortunate conditions: 1) Fully-developed, turbulent, constant pressure, jet mixing velocity profiles are the same for most gases, and even for low-viscosity liquids including water, and they are not functions of Mach number. This profile is well represented by the Gaussian error function. 2) The growth of the mixing layer is linear with length.

Figure 5 shows the jet mixing method. The fully developed velocity profile is shown on the right between two parallel, but opposite flows, U and U_B. The separating flow has a boundary layer. Hill and Page[14] devised a method for representing the effect of the boundary layer on the downstream profile. They replaced the boundary layer by a fictitious starting point for the jet mixing that would have the same displacement and momentum thickness at the actual separation plane as the real boundary layer. This condition leads to[15]

$$-\frac{\underline{\sigma}}{X_0}\delta_2 = \underline{\eta_e} - \underline{\eta_m} - \int_{-\infty}^{e} \frac{\rho}{\rho_e}\underline{\Phi}\,\mathrm{d}\underline{\eta} = \underline{\eta_e} - \underline{\eta_m} - \left(1 - Cr_e^2\right) J_{1e} \quad (1)$$

where

$$J_{1e} = \int_{-\infty}^{e} \frac{\underline{\Phi}}{1 - Cr_e^2\underline{\Phi}^2}\,\mathrm{d}\underline{\eta}$$

and where single-stream jet mixing is indicated by underscore. This location is termed the virtual origin, whose location is

$$Y_0 = \delta_1 + \delta_2, \qquad Y_0' = \delta_1' + \delta_2'$$

where δ_1 and δ_1' are displacement thicknesses and δ_2 and δ_2' are the momentum thicknesses.

Two coordinate sets originate at the virtual origin. X and Y coordinates can be thought of as the edge of the inviscid outer flow. X is parallel to nearby inviscid streamlines, such as e. The x and y coordinates belong to the viscous mixing layer. The x coordinate is the center of the jet mixing velocity profile where

$$u = \tfrac{1}{2}(U_e - |U_B|)$$

The shift of the x coordinate from the X is shown by y_m in Fig. 5.

Korst's theory[13] gives the isobaric, plane turbulent, single-stream jet mixing profile as

$$\underline{\Phi} = \frac{u}{U_e} = \frac{1}{2}[1 + \mathrm{erf}(\underline{\eta})], \qquad \underline{\eta} = \underline{\sigma}\frac{y}{x}$$

$$\mathrm{erf}(\underline{\eta}) = \frac{2}{\sqrt{\pi}}\int_{-\infty}^{\underline{\eta}} e^{-b^2}\,\mathrm{d}b$$

where $\underline{\sigma}$ is the jet spreading parameter and only an empirical value is required. It equals 12 for subsonic flow of many gases and varies with speed for supersonic flow. There is some disagreement among investigators, but the value used here for $Cr_e^2 \le 0.255$ is

$$\underline{\sigma} \cong 12$$

and for $Cr_e^2 \ge 0.255$ is

$$\underline{\sigma} = 47.1Cr^2$$

where Crocco number is defined as

$$Cr_e^2 = \frac{M_e^2}{[2/(\gamma-1)] + M_e^2} = \frac{U_e^2}{2c_pT_0} = 1 - \frac{T_e}{T_0}$$

For two-stream opposed flows, the single-stream spreading parameter σ is multiplied by

$$(1-\Phi_B)/(1+\Phi_B), \qquad \Phi_B = |u_B|/U_e$$

and the velocity profile is

$$\Phi = [(1-\Phi_B)/2] + [(1+\Phi_B)/2]\,\mathrm{erf}(\eta)$$

If gases in the two parallel streams have different total temperatures, or if they are different gases and, thus, have different physical properties, then these vary across the mixing region. If the turbulent viscosity is due to the mixing of gas particles, in the sense of the exchange coefficient, then the same phenomena transport heat and mass. Then velocity and total temperature have similar profiles. This says that $P_r = 1$:

$$\frac{T_0 - T_{0B}}{T_{0e} - T_{0B}} = \frac{\Phi + \Phi_B}{1+\Phi_B}, \qquad \frac{T_0}{T_{0e}} = \left(\frac{\Phi+\Phi_B}{1+\Phi_B}\right)\left(1 - \frac{T_{0B}}{T_{0e}}\right) + \frac{T_{0B}}{T_{0e}}$$

In the same way, the exchange of gas global transports the physical properties of the gases:

$$\frac{\Re}{\Re_e} = \left(\frac{\Phi+\Phi_B}{1+\Phi_B}\right)\left(1 - \frac{\Re_B}{\Re_e}\right) + \frac{\Re_B}{\Re_e}$$

$$\frac{\gamma}{\gamma_e} = \left(\frac{\Phi+\Phi_B}{1+\Phi_B}\right)\left(1 - \frac{\gamma_B}{\gamma_e}\right) + \frac{\gamma_B}{\gamma_e}$$

The nondimensional density then becomes

$$\frac{\rho}{\rho_e} = \frac{\Re_e}{\Re}\left[1 - \Phi^2 Cr_e^2 \frac{\gamma_e}{\gamma_e - 1}\frac{\gamma-1}{\gamma}\frac{T_{0e}}{T_0}\frac{\Re_e}{\Re}\right]^{-1}\left(\frac{T_{0e}}{T_0}\right)\left(1 - Cr_e^2\right)$$

$$Cr_e^2 = 1 - \frac{T_e}{T_{0e}}$$

The separating streamline s separates the mass flowing above the virtual origin from that entrained. The net mass transfer across the separating streamline is zero. The amount of mass flow above the virtual origin remains above the streamline s. Because this is a turbulent mixing region, mass is crossing the line constantly, but the net amount crossing is zero. This condition can be written as

$$\rho_e U_e (y_e - y_m) = \int_s^e \rho u \,\mathrm{d}y \tag{2}$$

After multiplying by σ/X_0 and dividing by $\rho_e U_e$, we will get

$$\eta_e - \eta_m = \int_s^e \frac{\rho}{\rho_e}\Phi \,\mathrm{d}\eta \tag{3}$$

However, η_e and η_m for two-stream mixing can be converted from $\underline{\eta_e}$ and $\underline{\eta_m}$ for single-stream mixing such that

$$\eta_e = \underline{\eta_e}[(1-\Phi_B)/(1+\Phi_B)], \qquad \eta_m = \underline{\eta_m}[(1-\Phi_B)/(1+\Phi_B)]$$

When Eq. (3) is substituted into Eq. (2), the following expression can be obtained for the subsonic jet:

$$0 = -\underline{\eta_e}\left(\frac{1-\Phi_B}{1+\Phi_B}\right) + \underline{\eta_m}\left(\frac{1-\Phi_B}{1+\Phi_B}\right) + \int_s^e \frac{\rho}{\rho_e}\Phi \,\mathrm{d}\eta$$

For the supersonic jet,

$$0 = -\underline{\eta'_{e'}}\left(\frac{1-\Phi'_B}{1+\Phi'_B}\right) + \underline{\eta'_{m'}}\left(\frac{1-\Phi'_B}{1+\Phi'_B}\right) + \int_{s'}^{e'} \frac{\rho'}{\rho'_{e'}}\Phi' \,\mathrm{d}\eta'$$

Now, when the momentum equation is considered for the flow below the streamline e at the virtual origin ($x = 0$) and downstream section at $x = X_0$,

$$\rho_e U_e^2 (\underline{y_e} - \underline{y_m}) = \int_{-\infty}^{e} \rho u^2 \,\mathrm{d}y$$

or

$$\underline{\eta_e} - \underline{\eta_m} = \left(1 - Cr_e^2\right)\int_{-\infty}^{e} \frac{\underline{\Phi^2}}{1 - Cr_e^2\underline{\Phi^2}}\,\mathrm{d}\underline{\eta}$$

$$\underline{\eta_e} - \underline{\eta_m} = \left(1 - Cr_e^2\right) J_{2e} \tag{4}$$

where

$$J_{2e} = \int_{-\infty}^{e} \frac{\underline{\Phi^2}}{1 - Cr_e^2\underline{\Phi^2}}\,\mathrm{d}\underline{\eta}$$

After comparing Eqs. (1) and (4), one can find virtual distance X_0 such as

$$X_0 = \frac{\underline{\sigma}\,\delta_2}{\left(1 - Cr_e^2\right)(J_{1e} - J_{2e})}, \qquad X'_0 = \frac{\underline{\sigma'}\delta'_2}{\left(1 - Cr_{e'}^{\prime 2}\right)(J'_{1e'} - J'_{2e'})}$$

III. Balance

A. Mass Balances

Figure 6 shows the mass conservations. The r and r' streamlines join at a saddle point at the end of the wake. Streamlines s and r form a corridor for air that will be recirculated to the base region,

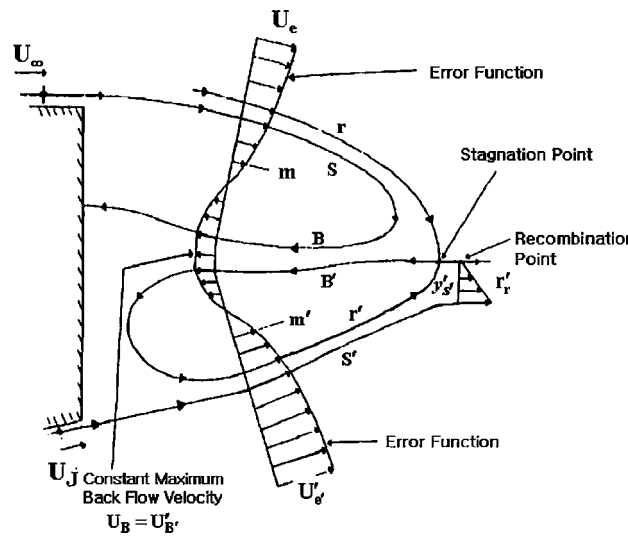

Fig. 6 Closed wake model.

and then r' and s' streamlines conduct this mass from the base to the downstream atmosphere. In general, when two freejet surfaces join in this manner, the stronger flow (higher total pressure) is the ejector, and the weaker is the feeder.

It is assumed that air is the gas in the corridor r–s, in the trapped vortex s–B, and in the corridor B–B'. From B to the jet exhaust stream, the gas is a mixture of air and engine exhaust gas. For the air regions, only T and P_0 vary across streamlines as functions of velocity Φ. For the mixed gas regions, T_0, γ, and $\Re$ also vary with Φ'. The density ratio for the airflow region simplifies to

$$\frac{\rho}{\rho_e} = \frac{1 - Cr_e^2}{1 - Cr_e^2\Phi^2}$$

Mass conservations are

$$2\pi \bar{R}_{r-s} \int_s^r \rho U \, \mathrm{d}y = 2\pi \bar{R}_{s'-r'} \int_{r'}^{s'} \rho' U' \, \mathrm{d}y'$$

$$= 2\pi \bar{R}_{B-B'} \int_{B'}^{B} \bar{\rho} U_B \, \mathrm{d}y$$

The bar indicates average value. Converting to dimensionless form, we have

$$\frac{\bar{X}}{\sigma} \bar{R}_{r-s} \rho_e U_e \int_s^r \frac{\rho}{\rho_e} \Phi \, \mathrm{d}\eta = \bar{R}_{s'-r'} \rho'_{e'} U'_{e'} \frac{\bar{X}'}{\sigma'} \int_{r'}^{s'} \frac{\rho'}{\rho'_{e'}} \Phi' \, \mathrm{d}\eta'$$

$$= \bar{R}_{B-B'} \bar{\rho}_B U_B (y_B - y_{B'}) \tag{5}$$

where

$$\bar{\rho}_B = \tfrac{1}{2}[\rho_B + \rho'_{B'}], \qquad \bar{X} = X_0 + 0.5L, \qquad \bar{X}' = X'_0 + 0.5L$$

The mass conservation is computed at the half distance plane of the wake. This is the end of the constant pressure portion (see the control volume in Fig. 7).

The first two equalities in Eq. (5) can be expressed as

$$\frac{\bar{R}_{r-s}}{\bar{R}_{s'-r'}} \frac{\sigma'}{\sigma} \frac{\bar{X}}{\bar{X}'} \frac{\rho_e}{\rho'_e} \frac{U_e}{U'_{e'}} \frac{1 - Cr_e^2}{1 - Cr_{e'}^2} = \frac{I'_{1s'}}{I_{1r}} \tag{6}$$

where r and r' streamlines join at a free stagnation point and, thus, must have equal total pressures as well as stream pressures equal to P_b:

$$P_r/P_{0r} = P_{r'}/P_{0r'}, \qquad (T_r/T_{0r})^{\gamma/(\gamma-1)} = (T_{r'}/T_{0r'})^{\gamma'/(\gamma'-1)}$$

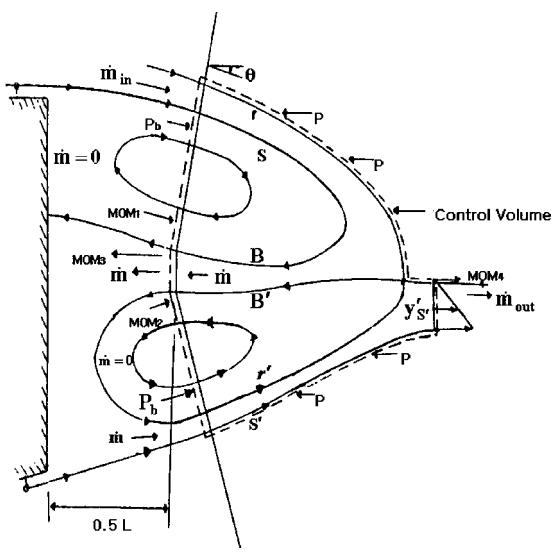

Fig. 7 Control volume for momentum and mass conservation.

However,

$$\frac{T}{T_0} = 1 - \frac{u^2}{2[\gamma/(\gamma-1)]\Re T_0}$$

or

$$\left[1 - \frac{\Phi_r^2 U_e^2}{2[\gamma/(\gamma-1)]\Re T_{0r}}\right]^{\gamma/(\gamma-1)}$$

$$= \left[1 - \frac{\Phi'^2_{r'} U'^2_{e'}}{2[(\gamma'/(\gamma'-1)]\Re' T'_{0r}}\right]^{\gamma'/(\gamma'-1)} \tag{7}$$

The first and third equalities in Eq. (5) yield

$$\frac{\bar{X}}{\sigma} \bar{R}_{r-s}\left(1 - Cr_e^2\right) \int_{\eta_s}^{\eta_r} \frac{\Phi}{1 - Cr_e^2\Phi^2} \, \mathrm{d}\eta = \bar{R}_{B-B'} \frac{\bar{\rho}_B}{\rho_e} \Phi_B \frac{\bar{X}}{\sigma} (\eta_B - \eta_{B'})$$

or

$$\bar{R}_{r-s}\left(1 - Cr_e^2\right)(I_{1r} - I_{1s}) = \bar{R}_{B-B'} \frac{\bar{\rho}_B}{\rho_e} \Phi_B (\eta_B - \eta_{B'})$$

$$\Phi_B = I_{1r} \frac{\bar{R}_{r-s}}{\bar{R}_{B-B'}} \frac{1 - Cr_e^2}{\eta_B - \eta_{B'}} \frac{\rho_e}{\bar{\rho}_B} \tag{8}$$

B. Momentum Balance

The control volume for satisfying the momentum equation is shown in Fig. 7. The momentum equation is

$$\sum F_{Ax} = \sum \dot{m}_{\text{out}} U_{Ax} - \sum \dot{m}_{\text{in}} U_{Ax}$$

where the subscript Ax indicates the axial direction. In the following development, θ is the angle between the streamline and nacelle axis. Because the control volume is bounded by streamlines on the top and bottom in Fig. 7, there are four momentum terms: 1) Mom_1 at midwake between B and r, 2) Mom_2 at midwake between B' and s', 3) Mom_3 at midwake between B and B', and 4) Mom_4 at downstream of wake between rr' and s':

$$\text{Mom}_1 = -2\pi \bar{R}_{B-r} \int_B^r \rho U^2 \, \mathrm{d}y(\cos\theta)$$

$$= -2\pi \bar{R}_{r-B} \frac{\bar{X}}{\sigma} \rho_e U_e^2 \left(1 - Cr_e^2\right) I_{2r} \cos\theta_r$$

$$\text{Mom}_2 = -2\pi \bar{R}_{B'-s'} \int_{B'}^{s'} \rho U^2 \, \mathrm{d}y(\cos\theta')$$

$$= -2\pi \bar{R}_{B'-s'} \frac{\bar{X}'}{\sigma'} \rho'_e U'^2_e \left(1 - Cr'^2_e\right) I_{2s'} \cos\theta_{s'}$$

$$\text{Mom}_3 = -2\pi \bar{R}_{B-B'} \bar{\rho}_B U_B^2 (y_B - y_{B'})$$

$$= -\pi \bar{R}_{B-B'} \Phi_B^2 \frac{\bar{X}}{\sigma} \rho_e U_e^2 \left(\frac{1 - Cr_e^2}{1 - Cr_e^2\Phi_B^2} + \frac{\rho_{B'}}{\rho_e}\right) (\eta_B - \eta_{B'})$$

$$\text{Mom}_4 = \frac{2}{3} \dot{m}_{B-B'} U_{\text{rec}} = \frac{2}{3}\left(-\frac{\text{Mom}_3}{\Phi_B U_e}\right) U_{\text{rec}}$$

The forces acting on the bubble are due to static pressure. Because both the streamlines r and s' are close to the inviscid wake surfaces, an assumption is made that the static pressure does not vary from streamline to streamline. Also, in the inviscid analysis, the pressure was assumed to be a function of X direction only in the wake region. Therefore, the surface force acting in the axial direction on the bubble is calculated by summing up the surface pressures on the bubble surface geometry used in the potential flow calculation:

$$\sum F_{AX} = 2\pi\left(R_{\bar{X}}^2 - R_{\bar{X}'}^2\right)P_b + 2\pi\sum_{i=k}^{N3}\frac{1}{2}(P_i + P_{i+1})(R_{i+1} - R_i) - 2\pi\sum_{i=k'}^{N3}\frac{1}{2}(P'_i + P'_{i+1})(R'_{i+1} - R'_i)$$

Thus,

$$\sum F_{Ax} = \mathrm{Mom}_1 + \mathrm{Mom}_2 + \mathrm{Mom}_3 + \mathrm{Mom}_4 \qquad (9)$$

C. Energy Balance

The control volume in Fig. 7 is also used for energy conservation computations. Energy transfer is done only by convection because the streamlines which boundaries have very small cross stream temperature gradients. All terms are of the form

$$\dot{E} = \int h_0\,\mathrm{d}\dot{m} = \int \frac{\gamma\Re}{\gamma - 1}T_0\rho U\,\mathrm{d}y \qquad \text{(energy/s)}$$

$$\sum E = \bar{R}_{B-r}\frac{\bar{X}}{\sigma}U_e\rho_e\frac{\gamma\bar{\Re}}{\gamma - 1}T_{0e}\left(1 - Cr_e^2\right)\int_B^r \frac{\Phi}{1 - Cr_e^2\Phi^2}\,\mathrm{d}\eta + \bar{R}_{B'-s'}\frac{\bar{X}'}{\sigma'}U'_e\rho'_e\int_{B'}^{s'}\frac{\gamma'\Re'}{\gamma' - 1}T'_0\frac{\rho'}{\rho'_e}\Phi'\,\mathrm{d}\eta' - \frac{\bar{X}}{\sigma}\bar{R}_{B-B'}U_e\Phi_B\bar{\rho}_B\bar{T}_{0_{B-B'}}\bar{c}_{p_{B-B'}}(\eta_B - \eta_{B'}) - \bar{R}_{rr'-s'}\dot{m}_{rr'-s'}\bar{c}_{p_{rr'-s'}}\bar{T}_{0_{rr'-s'}} = 0 \qquad (10)$$

where

$$m_{rr'-s'} = \mathrm{Mom}_3/\Phi_B U_e, \qquad T_{0_{rr'-s'}} = \tfrac{3}{4}T_{0e'} + \tfrac{1}{4}T_{0e}$$

$$\bar{\gamma} = \tfrac{3}{4}\gamma_{e'} + \tfrac{1}{4}\gamma_e, \qquad \bar{\Re} = \tfrac{3}{4}\Re_{e'} + \tfrac{1}{4}\Re_e$$

$$\bar{c}_{p_{rr'-s'}} = \{[(\bar{\gamma} - 1)/\bar{\gamma}]\bar{\Re}\}_{rr'-s'}, \qquad T_b = \tfrac{1}{2}(T_{0B} + T_{0B'})$$

If the $\sum E$ does not equal zero, $T_{0B'}$ is changed to satisfy the equation. The base temperature is then

$$T_b = \tfrac{1}{2}(T_{0B} + T_{0B'})$$

IV. Results and Discussion

Despite numerous inquires to research laboratories and engine manufacturers, no usable data were found to test this method in all of its capabilities: axisymmetric, both subsonic and supersonic, and with engine exhaust gas at high temperature and different from air. Figures 8–12 show predicted trends, and physical descriptions are provided as needed. The basic phenomenon is entrainment of air from the wake by the mass flux of the two streams, and so the values of $\rho_e u_e$ and $\rho'_{e'}u'_{e'}$ are the main criteria. For these, unless otherwise listed, $M_\infty = 0.6, M_J = 1.4, \theta_J = 10$ deg, $L/H = 2.0$, $\gamma = 1.31$, $\Re = 70[(ft - lb)/lb_m^\circ R]$, and $T_{0J} = 3T_{0\infty}$.

Figure 8 shows computed pressures with variable exhaust gas temperatures. It can be seen that base pressure P_b/P_∞ increases slightly with increasing jet stagnation temperature, mainly due to decreasing density. From this simple analysis, it is expected that there is much more air entrainment when air properties are used instead of the gas properties, and subsequently higher mass flux decreases the base pressure.

Figure 9 shows computed pressures with variable flight Mach numbers. It can be observed that the base pressure decreases with increasing flight Mach numbers. A simple justification is as follows. An increase in M_∞, corresponds to an increase in the velocity for constant atmospheric pressure and temperature. Therefore, it is expected that more air is entrained from the base region to the freestream and, thus, the higher mass flux at the base causes the base pressure to drop.

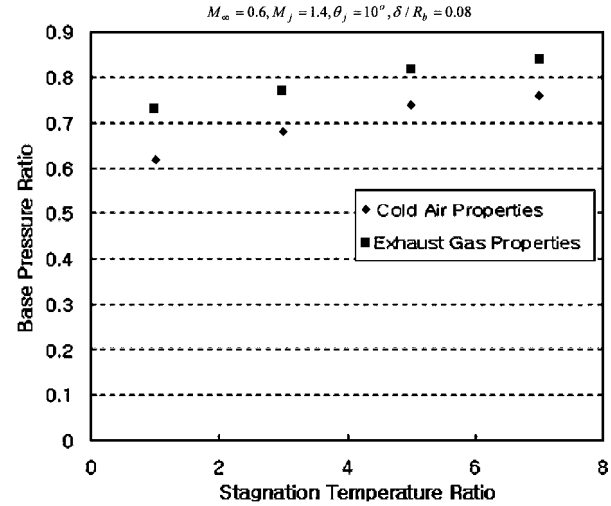

Fig. 8 Effect of stagnation temperature.

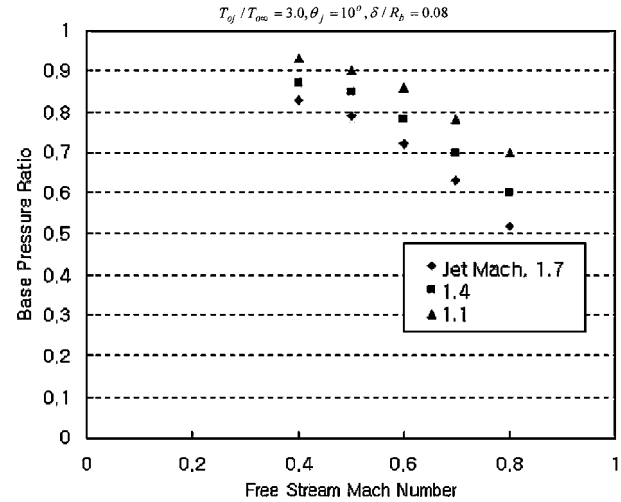

Fig. 9 Effect of flight Mach number.

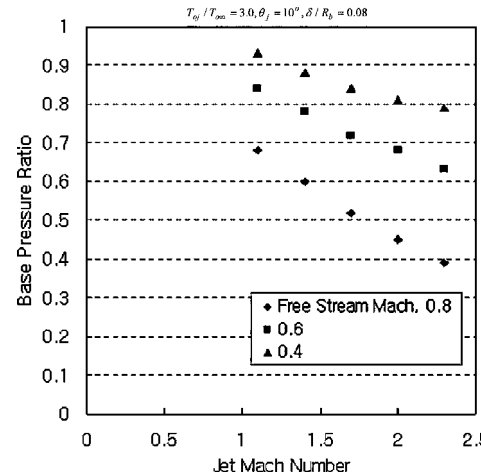

Fig. 10 Nozzle jet Mach number effect.

Figure 10 shows the computed base pressures with variable jet Mach numbers. Note that the base pressure decreases with increasing jet Mach number. The following analytical argument is the same as for Fig. 8.

Figure 11 shows computed base pressures with variable jet nozzle deflection angles. The trends were as expected from physical reasoning, and one can expect that base pressure will increase with increasing nozzle deflection angle θ_J.

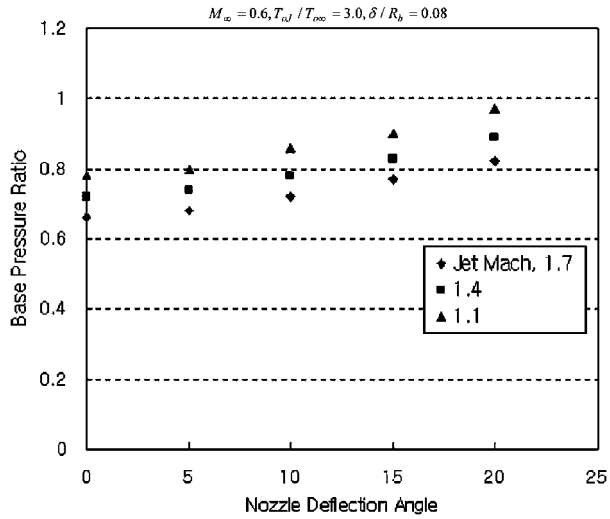

Fig. 11 Effect of nozzle deflection angle.

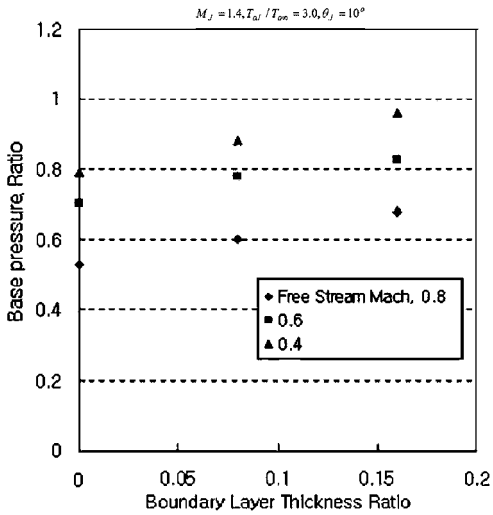

Fig. 12 Effect of boundary-layer thickness.

Figure 12 shows the effect of boundary-layer thickness. As expected, the base pressure increases with increasing boundary-layer thickness. Nearby flow, which does the entraining, is slow when the boundary layer is thick. The entrainment is a small amount, and a base pressure is not pulled down to a lower value. Therefore, thicker boundary layer makes base pressure higher.

It is interesting to compare the preceding results using air properties instead of exhaust gas properties. The results are shown in Fig. 8 and demonstrate that changing the jet gas physical properties results in base pressure reduction of 12%. We see that changing $T_{0J}/T_{0\infty}$ from 3 to 1 for a gas reduces P_b by 8%. If a wind-tunnel simulation uses cold air as the exhaust gas, both of the simplifications are being made. Computation of this condition gives $P_b/P_\infty = 0.62$, a 20% reduction. This is a warning for accepting such a simulation.

The wake length L is chosen at the start and seldom changed. Trial computations indicated that the wake length is not a very sensitive parameter (see Figs. 13 and 14). For $L/H = 2.0$ and 2.5, the base pressures P_b/P_∞ are 0.69 and 0.71, respectively.

Figure 15 shows experimental[16] and computed pressures for a boattailed nacelle tested in a wind tunnel with air in both streams and equal total temperatures on a circular arc boattail geometry, which is shown in Fig. 16. The afterbody pressure and base pressure are very well predicted for this attached flow, especially if a reasonable boundary-layer thickness is assumed. Figure 17 shows the streamline shape on the boattail wake.

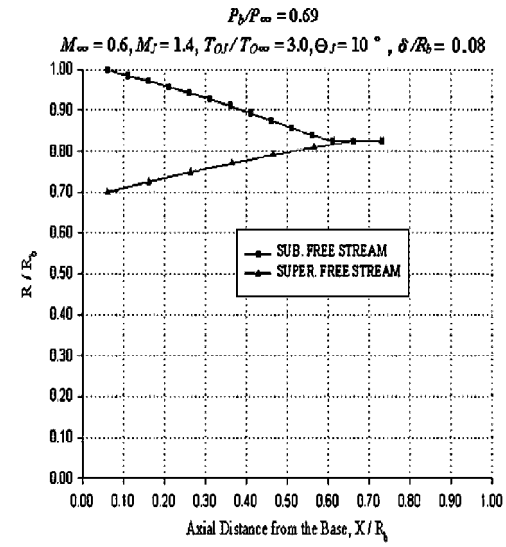

Fig. 13 Streamline shape for cylindrical nacelle, $L/H = 2.0$.

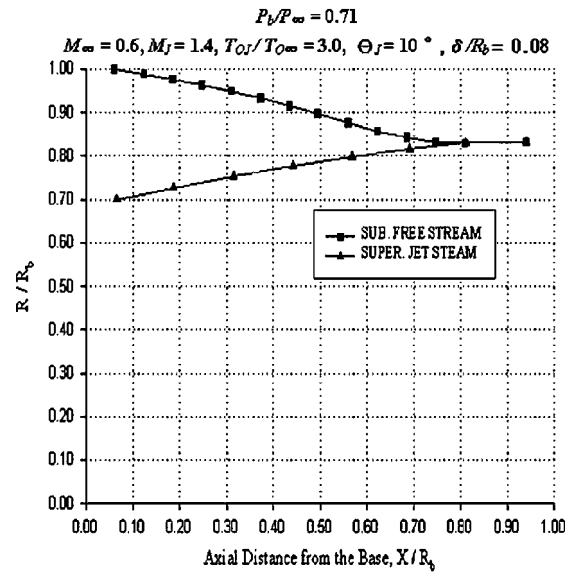

Fig. 14 Streamline shape for cylindrical nacelle, $L/H = 2.5$.

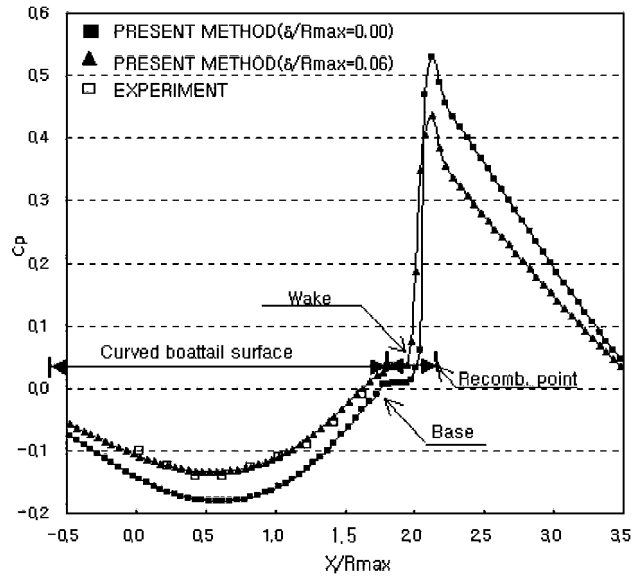

Fig. 15 Computed and experimental[16] pressure on boattail wake.

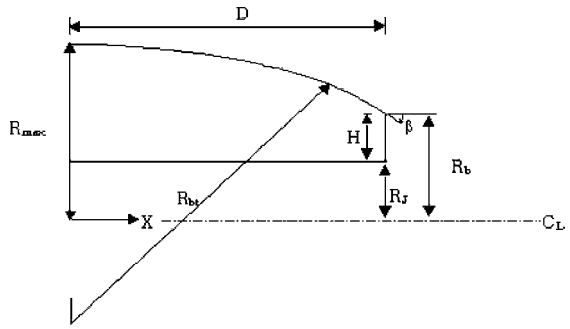

$D/R_{max} = 1.80$, $R_b/R_{max} = 0.62$, $R_J/R_{max} = 0.4$, $R_{bt}/R_{max} = 8.51$, and $\beta = 12.5$ deg.

Fig. 16 Circular arc boattail nacelle.[16]

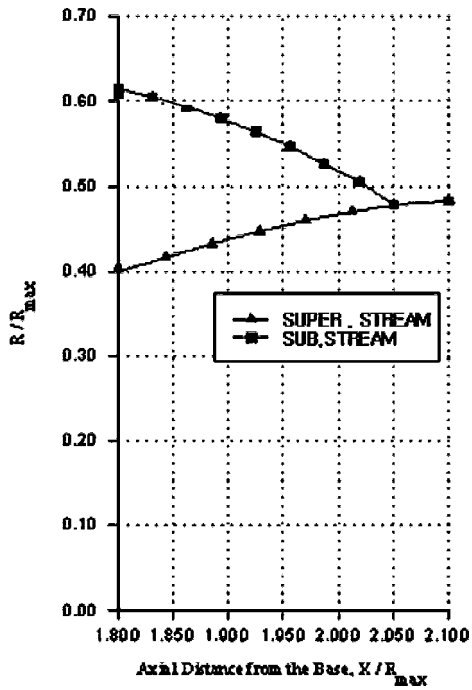

Fig. 17 Streamline shape on boattail wake.

V. Conclusions

A computer program has been developed to predict base flow for an annular base between sub- and supersonic flows of dissimilar gases. The nearly total lack of experimental data in the open literature precluded proper testing of the results. However, computed results are qualitatively correct; the expected physical conditions (wake shape, velocities of the major streamlines, base pressure ratio) are as expected. Even when excessively large initial values for the *r* and *s* streamlines are chosen, the program drives the solution to values which typically prevail for Korst mixing theory[13] applications.

For the one available data set, the results were in excellent agreement. Further computations will be performed to establish trends and, hopefully, test this method against experimental results.

Careful attention to the mass flow equations reveals that the stream with the largest mass flux tends to entrain the most mass from the wake. Thus, the temperature in the wake, which depends on which stream feeds the wake region, will be the stagnation temperature of the stream with the lower mass flux. This is determined mainly by being the one with the lower stagnation pressure. Rockets at very high speed often have combustion gases in their region, with resulting problems.

A recommendation for future work is the extension of the model to include three different mixing streams by adding another airflow between the streams considered here. This would then treat the fan-jet case or cooling air for an afterburner engine. Also, this analytical method can be applied easily to a rocket engine nozzle having a large base area.

References

[1]Holst, T., "Numerical Simulation of Axisymmetric Boattail Fields with Plume Simulators," AIAA Paper 77-224, Jan. 1977.

[2]Mikhail, A. G., "Computation of a Supersonic Flow Field Past an Axisymmetric Nozzle Boattail with Jet Exhaust," AIAA Paper 78-993, July 1978.

[3]Peery, K. M., and Forester, C. K., "Numerical Simulation of Multistream Nozzle Flows," AIAA Paper 79-1549, July 1979.

[4]Diewert, G. S., "Numerical Simulation of Three-Dimensional Boattail Afterbody Flowfield," AIAA Paper 80-1347, July 1980.

[5]Hasen, G. A., "Navier–Stokes Solutions for an Axisymmetric Nozzle," *AIAA Journal*, Vol. 20, No. 9, 1982, pp. 1219–1227.

[6]Korst, H. H., and Tripp, W., "The Pressure on a Blunt Trailing Edge Separating Two Supersonic Two-Dimensional Air Streams of Different Mach Numbers and Stagnation Pressures, but Identical Stagnation Temperatures," *Proceedings of Fifth Midwestern Conference on Fluid Mechanics*, Univ. of Michigan, Ann Arbor, MI, 1957, pp. 187–199.

[7]Page, R. H., and Korst, H. H., "Nonisoenergetic Turbulent Compressible Jet Mixing with Consideration of Its Influence on the Base Pressure Problem," *Proceedings of Fourth Midwestern Conference on Fluid Mechanics*, Purdue Univ., Sept. 1955, pp. 45–68.

[8]Dixon, R. J., and Page, R. H., "Turbulent Base Flow on an Axisymmetric Body with a Single Exhaust Jet," *Journal of Aircraft*, Vol. 7, No. 7, 1970, pp. 848–854.

[9]Izadi, M. J., "Computational Fluid Dynamics of the Base Flow on a Plane Body Between a Subsonic Flow on One Side and a Supersonic Flow on the Other," Ph.D. Dissertation, Aerospace Engineering Dept., Wichita State Univ., Wichita, KS, May 1991.

[10]Shapiro, A. H., *The Dynamics and Thermodynamics of Compressible Fluid Flow*, Vol. 1, Wiley, New York, 1953.

[11]Kuchemann, D., *Aerodynamics of Propulsion*, McGraw–Hill, New York, 1953, pp. 305–316.

[12]Tam, C., Jackson, J., and Seiner, J., "A Multiple-Scales Model of the Shock-Cell Structure of Imperfectly Expended Supersonic Jets," *Journal of Fluid Mechanics*, Vol. 153, 1985, pp. 123–149.

[13]Korst, H. H., "A Theory for Base Pressures in Transonic and Supersonic Flow," *Journal of Applied Mechanics*, Vol. 23, No. 4, 1956, pp. 593–600.

[14]Hill, W. G., and Page, R. H., "Initial Development of Turbulent, Compressible Free Shear Layer," *Journal of Basic Engineering*, Vol. 91, Ser. D, No. 1, 1969, pp. 120–122.

[15]Baik, D. S., "Computation of the Base Flow for an Axi-Symmetric Nacelle Configuration," Ph.D. Dissertation, Aerospace Engineering Dept., Wichita State Univ., Wichita, KS, May 1997.

[16]Peace, A. J., "Turbulent Flow Predictions for Afterbody/Nozzle Geometries Including Base Effects," *Journal of Propulsion*, Vol. 7, No. 3, 1991, pp. 396–403.